Microchimica Acta (2022) 189:427
https://doi.org/10.1007/s00604-022-05525-w

ORIGINAL PAPER

Sensitive colorimetric assay of hydrogen peroxide and glucose in humoral samples based on the enhanced peroxidase-mimetic activity of NH_2-MIL-88-derived FeS_2@CN nanocomposites compared to its precursors

Ru Fan[1] · Jinrong Tian[1] · Huili Wang[2] · Xuedong Wang[2] · Peipei Zhou[1]

Received: 8 July 2022 / Accepted: 30 September 2022 / Published online: 19 October 2022

Abstract

By employing NH_2-MIL-88 as a template, we synthesized the intermediate Fe@CN under high-temperature calcination and further fabricated the FeS_2@CN nanocomposites in the presence of sulfur powder. Under varying temperatures (300–600 °C) and Fe@CN-to-S ratios (1:3–6), $FeS_2@CN_{500\text{-}5}$ nanocomposites had the highest peroxidase-mimetic activity. Under optimized conditions (incubation temperature 40 °C; solution pH 4.0 and nanocomposite concentration 10 μg/mL; 652-nm absorption), the Michaelis-Menten constant (K_m) of FeS_2@CN was much lower than that of horseradish peroxidase (HRP), therefore demonstrating that it had a higher affinity for both chromogenic substrates than conventional HRP. The limits of detection for H_2O_2 and glucose were 0.15 and 0.30 μmol/L, respectively, and the recoveries for glucose were 91.8–103% with RSDs <5.2%. The novelty of this study lies in (1) the FeS_2@CN was confirmed to possess stronger enzyme-mimetic activity than its precursors (NH_2-MIL-88 and Fe@CN); (2) the enhanced activity resulted from the unsaturated sites of N and S doping and the plentiful defects on the porous carbon surface; and (3) free radical trapping experiments evidenced that •OH played a major role in the catalytic reaction, while h^+ and $•O_2^-$ simultaneously participated in the catalytic process. These convincing performance metrics lead us to postulate that the FeS_2@CN-based colorimetric biosensor provides a promising approach for several real-world applications, such as point-of-care diagnosis and workplace health evaluations.

Keywords FeS_2@CN · Reaction precursors (NH_2-MIL-88 and Fe@CN) · Nanozymic activity · Colorimetric sensor · ROS trapping · Glucose · Hydrogen peroxide

Introduction

Metal-organic frameworks (MOFs) belong to a type of crystalline inorganic-organic framework of nanohybrids, which consist of metal ions or clusters that form a three-dimensional network [1, 2]. MOFs often have a large, uniform surface area and pore volume, and their physical properties can be changed with varying synthetic conditions [3]. Consequently, they are often considered as an ideal template for preparing porous carbon structures as their surfaces are easily functionalized under mild conditions [4]. To date, MOFs have been widely used in many fields, including adsorption [5], separation [6], and gas storage [7]. However, MOFs often show instability and low efficiency in the catalytic reaction to a certain degree [8]. This limits the scope of their applications, especially in the colorimetric assay of biomacromolecules based on the chromogenic reaction of 3,3′,5,5′-tetramethylbenzidine (TMB) to 3,3′,5,5′-tetramethyldiphenone (TMB_{ox}).

The development of nanocomposites, with highly catalytic capacity and stability, and good biocompatibility, is of great importance to the nano-regulation of surface components and physicochemical properties

✉ Xuedong Wang
zjuwxd@163.com

✉ Peipei Zhou
zhoupeipei345@126.com

[1] Zhejiang Provincial Key Laboratory of Watershed Science and Health, College of Public Health and Management, Wenzhou Medical University, Wenzhou 325035, China

[2] School of Environmental Science and Engineering, Suzhou University of Science and Technology, Suzhou 215009, China

[9–11]. To date, it has been a more popular approach to fabricate nanocomposites by combining specific high-surface-area MOFs with transition metal oxides (TMO) and/or sulfides (TMS). For instance, several types of carbon templates are introduced to fabricate composites, such as carbon nanotubes (SnS_2-CNTs) [12], carbon nanofibers (WS_2@NCNFs) [13], and porous carbon (MoS_2@CMK-3) [14]. Overall, the inherent chemical merits and external structure design of nanocomposites could both influence the enzyme-like activity in those works. Shao et al. (2018) designed a MOFs-derived triple-component composite (FeS_2, N, S-codoped porous carbon, and rGO) with a high rate of sodium-ion storage ability [15]. So far, there is a paucity of information regarding the nanozymic activity of MOFs-derived TMS (MOFs@TMS). Motivated by the previous research circumstances, we fabricated an NH_2-MIL-88-derived porous carbon nanohybrid (FeS_2@CN) for unraveling its peroxidase-like activity.

Hydrogen peroxide (H_2O_2) is an important bioactive molecule in biological systems, and glucose is the key energy source of human daily activity [16–19]. Consequently, it is of great significance to develop efficient and sensitive assay techniques for both H_2O_2 and glucose in biological research and point-of-care diagnosis. Among previously reported methods, colorimetric detection based on horseradish peroxidase (HRP) has attracted much attention because of its simplicity, rapidity, small background interference, and high sensitivity [20]. However, as a natural enzyme, HRP is expensive to prepare and not easily stored after denaturation, heating, or chemical changes [21]. In recent years, novel nanozymes with peroxidase-like activity have been developed as alternatives to address the issues associated with natural enzymes, such as high cost, and storage difficulties. It is worth noting that their applications in the detection of glucose and H_2O_2 have become a research hotspot [22].

Building upon previous studies, we employed NH_2-MIL-88 as a template of porous carbon structure and then introduced sulfur powder into the template for the sake of fabricating shuttle-like FeS_2@CN nanohybrids under the calcining conditions. The NH_2-MIL-88-derived FeS_2@CN nanohybrids not only inherit some basic advantages of MOFs, such as large specific surface area and high porosity, but also possess better stability and higher activity due to the presence of more active sites than its precursors, FeS_2 and NH_2-MIL-88. Subsequently, a series of experiments were conducted to investigate the catalytic performance of as-fabricated FeS_2@CN nanohybrids for glucose and H_2O_2 by virtue of the chromogenic reaction from colorless TMB to blue TMBox (Fig. 1). Also, we optimized in detail the important reaction variables and rigorously studied the anti-interference effects of as-constructed colorimetric biosensors. This shuttle-like FeS_2@CN nanomaterial was confirmed to have strong peroxidase-mimetic activity and could be satisfactorily applied for H_2O_2 and glucose assay in the humoral samples.

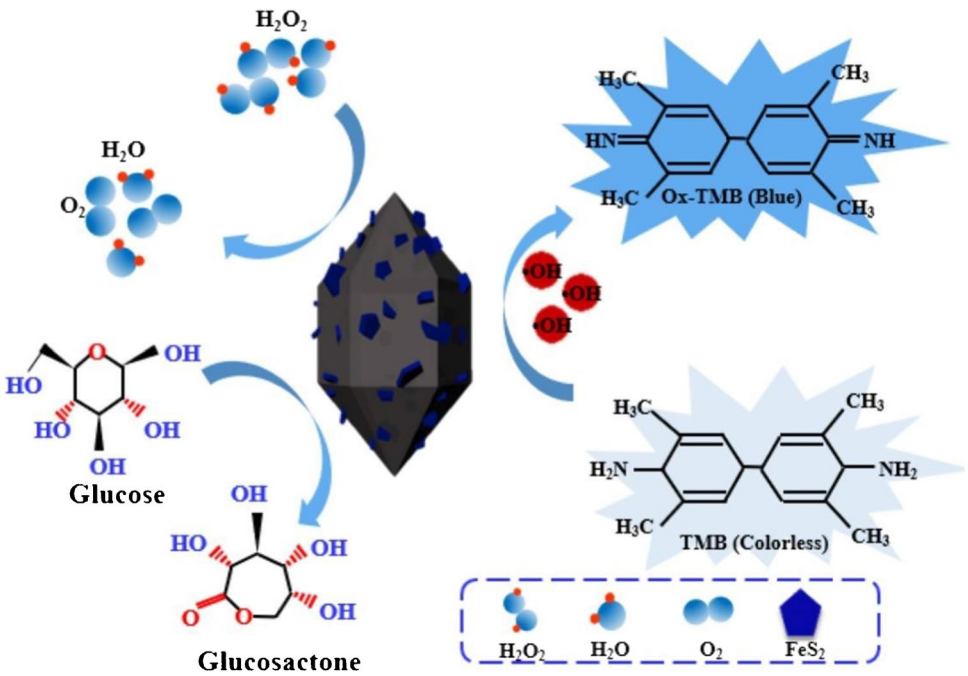

Fig. 1 Schematic illustration of FeS_2@CN as a peroxidase for H_2O_2 detection

Experimental

Reagents

All chemicals employed in this study were of analytical grade and used when received without further purification. A series of chemicals were purchased from Aladdin (Shanghai, China), which included TMB, ethanol, ferric nitrate hexahydrate ($Fe(NO)_3 \bullet 9H_2O$,>99%), 4-nitrophenyl acetic acid ($C_8H_7NO_4$,>99%), hydrogen peroxide (H_2O_2, 30%), sodium acetate (NaAC,>99%), sublimated sulfur, glucose, N, N-dimethylformamide (DMF, 98%), and dimethyl sulfoxide (DMSO, ≥95%). Ultrapure water (>18.2 MΩ) was generated with a Milli-Q gradient system (Bedford, MA, USA).

Instruments

Powder X-ray diffraction (XRD) patterns of the FeS_2@CN material were determined using a Bruker D8 Advance X-ray diffractometer (Bruker, Billerica, MA, USA) with Cu Kα radiation (λ = 0.15418 nm). The morphology of FeS_2@CN was characterized by a high-angle annular dark-field scanning transmission electron microscopy (TEM, TALOS F200S, FEI, USA). X-ray photoelectron spectroscopy (XPS) was measured on a Thermo ESCALAB 250Xi (Thermo Fisher Scientific, Waltham, MA, USA) with a monochromatic Al Kα source. Fourier transform infrared (FT-IR) spectra were determined using a Thermo Fisher Scientific IS5 (Waltham, MA, USA). UV-visible spectra were recorded using a Shimadzu UV-260 spectrophotometer (Tokyo, Japan).

Synthesis of FeS_2@CN

Synthesis of NH_2-MIL-88 (Fe)

NH_2-MIL-88 (Fe) was synthesized by a facile one-step hydrothermal method [15]. Briefly, 1.33 g of $Fe(NO)_3 \bullet 9H_2O$ and 0.71 g of 2-aminoterephthalic acid were dissolved in 100 mL of N, N-dimethylformamide (DMF) to form 0.33 mol/L solutions A and B, respectively. Then, aliquots of solution A (15 mL) and solution B (15 mL) were homogeneously mixed and transferred to a 100-mL stainless steel autoclave and heated at 120 °C for 24 h. After the autoclave was cooled to room temperature, the resultant material was washed three times with DMF and ethanol and then dried in a vacuum dry oven at 80 °C for 24 h. Finally, the dark black material, i.e., NH_2-MIL-88(Fe), was sealed and stored at ambient conditions for subsequent use.

Synthesis of Fe@CN

The quartz boat filled with NH_2-MIL-88(Fe) powder was placed in a tube furnace, and N_2 flow was introduced for 20 min to discharge the air in the tube. Then, the NH_2-MIL-88(Fe) powder was heated at 600 °C for 2 h and an N_2 atmosphere with a heating rate of 5 °C/min. After the tubular furnace was cooled to room temperature, the calcined powder was taken out and washed with water and ethanol three times. Finally, the resulting dark black product (Fe@CN) was dried in a vacuum oven at 60 °C for 6 h, ground and sealed for later use.

Synthesis of FeS_2@CN

The as-fabricated Fe@CN powder was uniformly mixed with sublimed sulfur at a series of mass ratios, and the mixture was placed in a quartz boat. This was then calcined in a tubular furnace at 500 °C for 2 h with a heating rate of 5 °C/min and an N_2 atmosphere. Prior to calcining, the N_2 flow was preliminarily blown for 20 min to drive out the air. After the tubular furnace was cooled to room temperature, the calcined powder was taken out and washed with water and ethanol three times. Finally, the acquired dark gray powder (FeS_2@CN) was dried in a vacuum oven at 60 ℃ for 6 h, ground and sealed for later use.

Optimization of the synthetic conditions

Effect of temperature

After the Fe@CN was successfully synthesized, it was mixed with sublimed sulfur powder at the ratio of 1:5 (w/w). The subsequent calcining procedure was set at a series of temperatures (300, 400, 500, and 600 °C) for 2 h at a gradient rising rate of 5 °C/min. The effect of temperature was evaluated by testing the peroxidase-like activity of the FeS_2@CN nanocomposite to catalyze colorless TMB into blue TMBox.

Optimization of sulfur powder quantity

To assess the effect of sulfur power quantity, a series of mass ratios of Fe@CN to sublimed sulfur were set at 1:3, 1:4, 1:5, and 1:6, respectively, with the synthetic procedures as detailed in the "Synthesis of FeS_2@CN" section. Finally, all the fabricated nanomaterials were tested for their respective peroxidase-like activities based on the optical densities (ODs) at 652 nm, and the optimal amount of sulfur powder was selected in final test.

The peroxidase-like activity of FeS_2@CN nanocomposite

The peroxidase-like activity of the as-fabricated nanomaterial was determined by catalyzing the oxidation of TMB in the presence of H_2O_2. Under optimized conditions, varying levels of H_2O_2 (0.01–0.80 mmol/L) or TMB (0.1–1.6 mmol/L) were added to carry out the steady-state kinetic experiments. In brief, 50 μL of 1 mg/mL FeS_2@CN suspension was added to 1710 μL of NaAc-HAc buffer solution (20 mmol/L, solution pH 4.0). Then, 200 μL of 6 mmol/L TMB and 40 μL of 150 mmol/L H_2O_2 were sequentially added to the mixed solution outlined above. The mixed solution was then incubated at 40 °C for ~20 min until a blue solution formed. The supernatant was purified by a 0.22-μm microporous membrane after the reaction was over, and the 652-nm ODs of the filtered solution was measured by a spectrophotometer. Finally, the enzymatic reaction constants (V_{max} and K_m) were calculated based on the Michaelis-Menten equation (1), which describes the relationship between the conversion rate of a given substrate and the substrate concentration of an enzyme (FeS_2@CN in this case):

$$\frac{1}{V} = \left(\frac{K_m}{V_{max}}\right) * \left(\frac{1}{[S]}\right) + \frac{1}{V_{max}} \quad (1)$$

where K_m is the Michaelis-Menten constant, $V_{\max}$ is maximum reaction velocity, and *[S]* is TMB concentration [23].

Colorimetric assay of H_2O_2 and glucose

To acquire the calibration plot of H_2O_2, 50 μL of 1 mg/mL FeS_2@CN, 200 μL of 6 mmol/L TMB solution, 40 μL of H_2O_2 aqueous solution with different concentrations (0.1–100 μmol/L), and 1710 μL of 20 mmol/L NaAc-HAc buffer solution (pH 4.0) were added to a quartz cuvette. Then, the mixed solution was incubated at 40 °C for ~20 min. Finally, the 652-nm ODs of filtered supernatant was measured by a spectrophotometer.

For the sake of acquiring the linear relationship of glucose, 100 μL of 0.5–150 μmol/L glucose and 50 μL of 2 mg/mL glucose oxidase were added to 100 μL of 20 mmol/L NaAc-HAc buffer solution (pH 7.0), and then the mixed solution was incubated at 40 °C for 30 min. After that, 200 μL of 6 mmol/L TMB, 50 μL of 1 mg/mL FeS_2@CN, and 1500 μL of 20 mmol/L NaAc-HAc buffer solution (pH 4.0) were added to the aforementioned reaction solution, incubated at 40 °C for 20 min and detected by a spectrophotometer.

H_2O_2 and glucose assay in human serum samples

Human serum samples were gratis supplied by the Department of Clinical Laboratory at the First Affiliated Hospital of Wenzhou Medical University, Wenzhou, China. These samples were collected from 5 male and 5 female healthy volunteers with an average age of 30±5 and then stored at −80 °C. Prior to analysis, the frozen samples were thawed at 4 °C and then centrifuged at 10,000 rpm for 20 min to remove large aggregates. Hereafter, the supernatant was diluted 200-fold with NaAc-HAc buffer (20 mmol/L, pH 7.0) to obtain the as-pretreated serum samples. Subsequently, 100 μL of serum sample and 50 μL of 2 mg/mL glucose oxidase were added to 100 μL of 20 mmol/L NaAc-HAc buffer solution (pH 7.0) and incubated at 40 °C for 30 min. Finally, 200 μL of 6 mmol/L of TMB, 50 μL of 1 mg/mL FeS_2@CN, and 1500 μL of 20 mmol/L NaAc-HAc buffer solution (pH 4.0) were added to the as-pretreated serum solution and incubated at 40 °C for 20 min. The supernatant was used for glucose quantification according to the above-constructed calibration plot.

Results and discussion

Optimization of material synthesis

As detailed in the "Optimization of the synthetic conditions" section, four gradient calcination temperatures (300–600 °C) were set for the fabrication of FeS_2@CN, and the corresponding nanocomposites are hereafter referred to as $FeS_2@CN_{300}$ for 300 °C, $FeS_2@CN_{400}$ for 400 °C, $FeS_2@CN_{500}$ for 500 °C, and $FeS_2@CN_{600}$ for 600 °C, respectively. Following the addition of TMB and H_2O_2 solution, a bright blue suspension appeared. As can be seen from Fig. S1A, the average ODs of $FeS_2@CN_{500}$ (n=3) reached as high as 1.39 a.u. followed by the addition of $FeS_2@CN_{400}$ and $FeS_2@CN_{600}$. In stark contrast, the $FeS_2@CN_{300}$ gave the lowest average ODs (0.74 a.u.). These results demonstrate that too low or high temperatures were not conducive to the enhancement of FeS_2@CN's peroxidase-like activity. Therefore, we selected the optimal synthesis temperature of 500 °C in subsequent trials.

The as-fabricated nanocomposites were designated as $FeS_2@CN_3$, $FeS_2@CN_4$, $FeS_2@CN_5$, and $FeS_2@CN_6$, respectively, at the fortified mass ratios of Fe@CN to sublimed sulfur powder of 1:3, 1:4, 1:5, and 1:6. Upon the addition of TMB and H_2O_2 solutions, a bright blue suspension appeared immediately. Obviously, the $FeS_2@CN_5$ provided the highest absorption intensity (Fig. S1B); on the contrary, the $FeS_2@CN_3$ gave the lowest ODs (0.62 a.u.) among the four nanocomposites. These findings provide strong evidence that 1:5 is the appropriate mass ratio of Fe@CN to sublimed sulfur powder for high peroxidase-like activity.

Characterization of the synthesized nanocomposites

We chose NH_2-MIL-88 (Fe) and sublimed sulfur powder as the precursors for the preparation of nanocomposites because the former could supply hierarchical pores and the latter could form rich doping defects. Figure 2A presents an the overall conceptual representation for the preparation of FeS_2@CN after carbonization and sulfidation, and the detailed procedures are described in the "Synthesis of FeS_2@CN" section. Clearly, the precursor NH_2-MIL-88(Fe) displayed a shuttle-like morphology (Fig. 2B and C). After annealing at 500 °C, Fe@CN could be obtained (Fig. 2E) and its shuttle-like morphology did not vary much although Fe atoms were observed to cover on the surface of porous carbon frameworks (Fig. 2D and E). As anticipated, the morphology of FeS_2@CN showed that the FeS_2 nanoparticles uniformly mosaic in shuttle-like carbon-based frameworks (Fig. 2F and G).

As for the FT-IR spectra of NH_2-MIL-88, Fe@CN, and FeS_2@CN (Fig. 3A), the broad band at 3150 cm^{-1} resulted from the O-H stretching vibration in amorphous carbon. The peaks at ~1570 cm^{-1} were attributable to the symmetric and asymmetric C=O vibrations, while those at 1050 and 992 cm^{-1} were assigned to aromatic C-N bonds [24]. Moreover, the tensile vibration peak at 510 cm^{-1} confirmed the existence of S-C in sulfide products [25]. In contrast to the NH_2-MIL-88, the disappearance of some characteristic bands in the FeS_2@CN demonstrated that, after carbonization and sulfidation, the chemical structure of NH_2-MIL-88 varied substantially [26].

XPS analyses were conducted to further characterize the surface component properties of NH_2-MIL-88, Fe@CN, and FeS_2@CN. As detailed in Fig. 3B, the FeS_2@CN was composed of C, S, Fe, O, and N, but no S peak was observed in both Fe@CN and NH_2-MIL-88. Additionally, the high-resolution C spectrum could be deconvoluted into three main sub-peaks, i.e., C-C/C=C (282.9 eV), C-N (283.8 eV), and C-S (285.7 eV), documenting that the as-fabricated nanocomposites contained sulfur (Fig. S2A). Figure S2B illustrates that there are various kinds of doped N, such as pyridinic N (396.5 eV), nitrile N (398.7 eV), and pyrrole N (400.9 eV) [15]. The XPS spectrum of Fe 2p (Fig. 3C) exhibited peaks at binding energies of 706.2 eV (Fe 2p3/2) and 723 eV (Fe 2p1/2), as well as peaks at 707.5 and 712.3 eV as FeS_2 and FeO, respectively [27, 28]. With regard to the chemical states of sulfur (Fig. 3D), five distinct sub-peaks were observed as follows: 168.3 eV (SO_x), 166.7 eV (C-S 2p1/2), 162 eV (C-S 2p3/2), 163.1 eV (S 2p1/2 of FeS_2), and 160.4 eV (S 2P3/2 of FeS_2). These unsaturated sites of N and S on the surface of porous carbon frameworks were both conducive to the enhancement of nanzymic catalytic capacity [25]. Other characterization details and figures of FeS_2@CN are described in the Electronic Supp. Material (ESM).

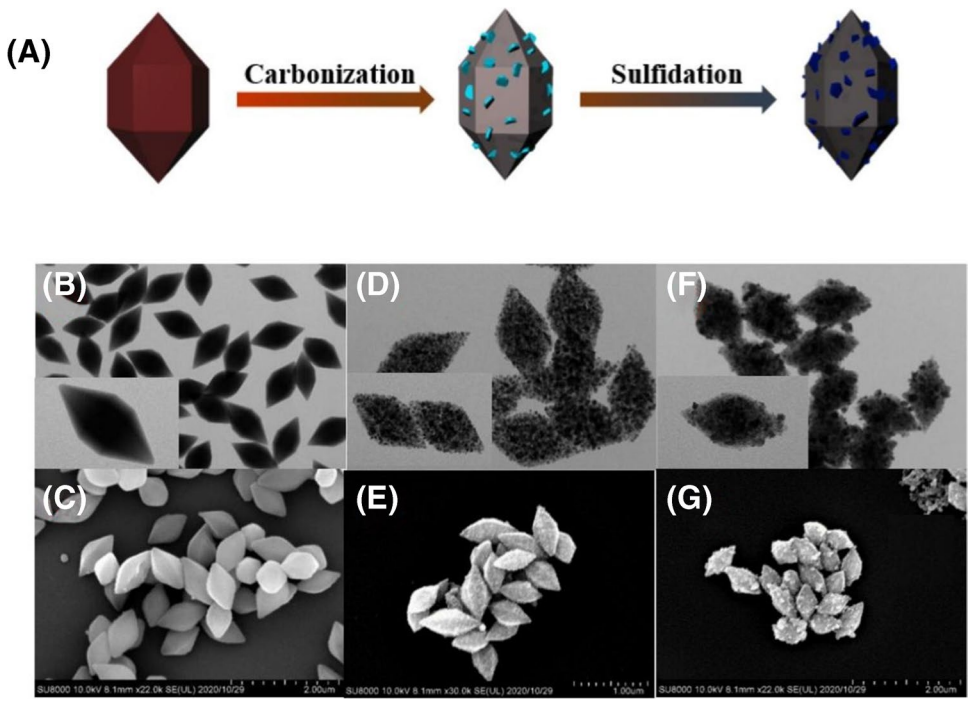

Fig. 2 Schematic diagram of the fabrication process of FeS_2@CN. TEM and SEM images of **B**, **C**: NH_2-MIL-88; **D**, **E**: Fe@CN; **F**, **G**: FeS_2@CN.

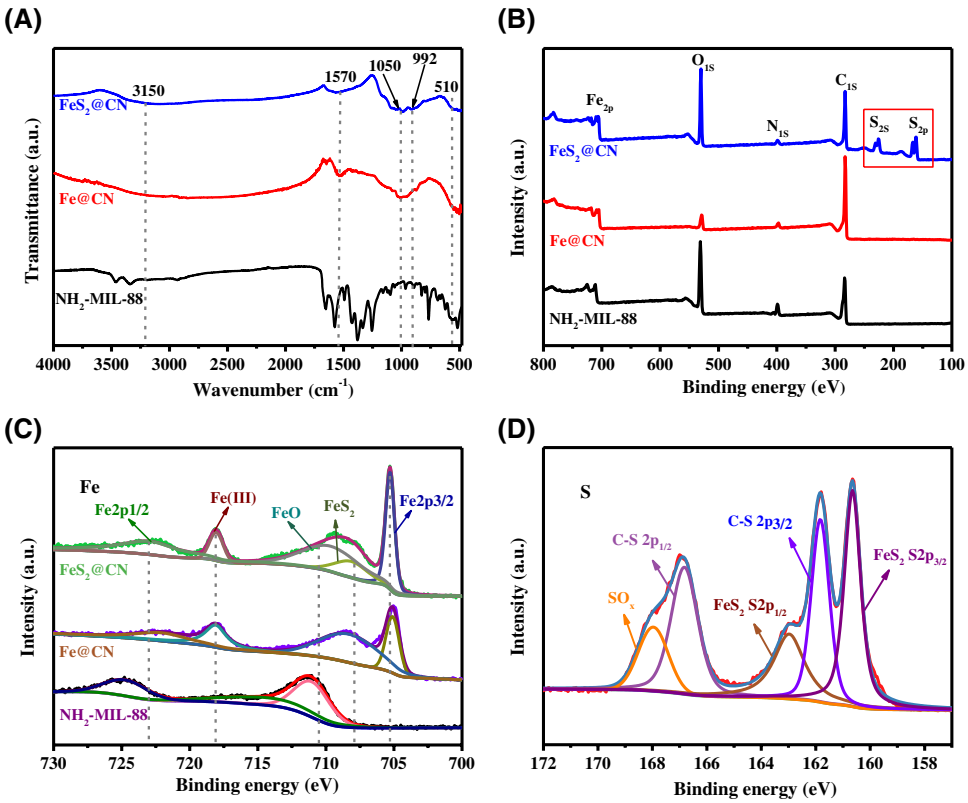

Fig. 3 **A** The FTIR spectra of NH_2-MIL-88, Fe@CN, FeS_2@CN. **B** The XPS spectra of NH_2-MIL-88, Fe@CN, FeS_2@CN. **C** High-resolution XPS spectra for Fe 2p NH_2-MIL-88, Fe@CN, FeS_2@CN. **D** High resolution XPS spectra for S 2p of FeS_2@CN.

Peroxidase-mimetic activities of three nanomaterials

To evaluate the peroxidase-mimetic activities of as-fabricated nanomaterials, we adopted TMB as a chromogenic substrate in the presence of H_2O_2. TMB was easily oxidized into TMBox in the H_2O_2/NH_2-MIL-88, H_2O_2/Fe@CN, and H_2O_2/FeS_2@CN systems, forming a bright blue suspension with a specific absorption at 652 nm. It can be clearly seen from Fig. 4A that the absorption intensity (1.39 a.u.) in the H_2O_2/FeS_2@CN system was much higher than those in the H_2O_2/NH_2-MIL-88 system (0.69 a.u.) and H_2O_2/Fe@CN system (0.08 a.u.). These findings evidence that the peroxidase-mimetic activity of as-fabricated nanocomposites was dramatically enhanced as compared to its precursors (NH_2-MIL-88 and Fe@CN), possibly resulting from the unsaturated sites of N and S, as well as the plentiful defects on the porous carbon surface.

Optimization of the important variables

As the peroxidase-like activity is closely dependent on experimental parameters, we rigorously investigated the effects of incubation temperature, solution pH, and initial concentration on the activity of FeS_2@CN. As displayed in Fig. 4B, the 652-nm ODs gradually increased from 0.83 to 1.39 a.u. in the FeS_2@CN/H_2O_2/TMB system when the incubation temperature ascended from 25 to 40 °C. However, when the temperature increased from 40 to 60 ℃, the absorbance gradually dropped to 0.5 a.u. (Fig. 4B). As a consequence, the highest peroxidase-like activity of FeS_2@CN occurred at 40 °C. As for solution pH, the 652-nm ODs sharply increased to 1.59 a.u. with increasing solution pH from 2.0 to 4.0, but decreased dramatically to 0.31 with the further increase to pH 5.0 (Fig. 4C). This phenomenon highlighted that the FeS_2@CN nanocomposites possessed the highest Fenton-like reaction activity in the pH range of 3.0–4.0. Moreover, when the initial concentration of FeS_2@CN increased from 0 to 10 μg/mL, the absorbance rapidly ascended to 1.93 a.u. Afterwards, the 652-nm ODs increased gradually from 1.93 to 2.27 a.u. as the fortified level of FeS_2@CN varied from 10 to 20 μg/mL. However, when it rose from 20 to 50 μg/mL, the absorbance remained nearly unchanged (Fig. 4D). Notably, when the ODs were >2.0, too high absorption was not beneficial for accurate quantification of target analytes. Based on the above-mentioned considerations, 10 μg/mL was adopted in the following experimental trials. In summary, three key variables were optimized as follows: incubation temperature, 40 °C; solution, pH 4.0; and nanocomposite concentration, 10 μg/mL.

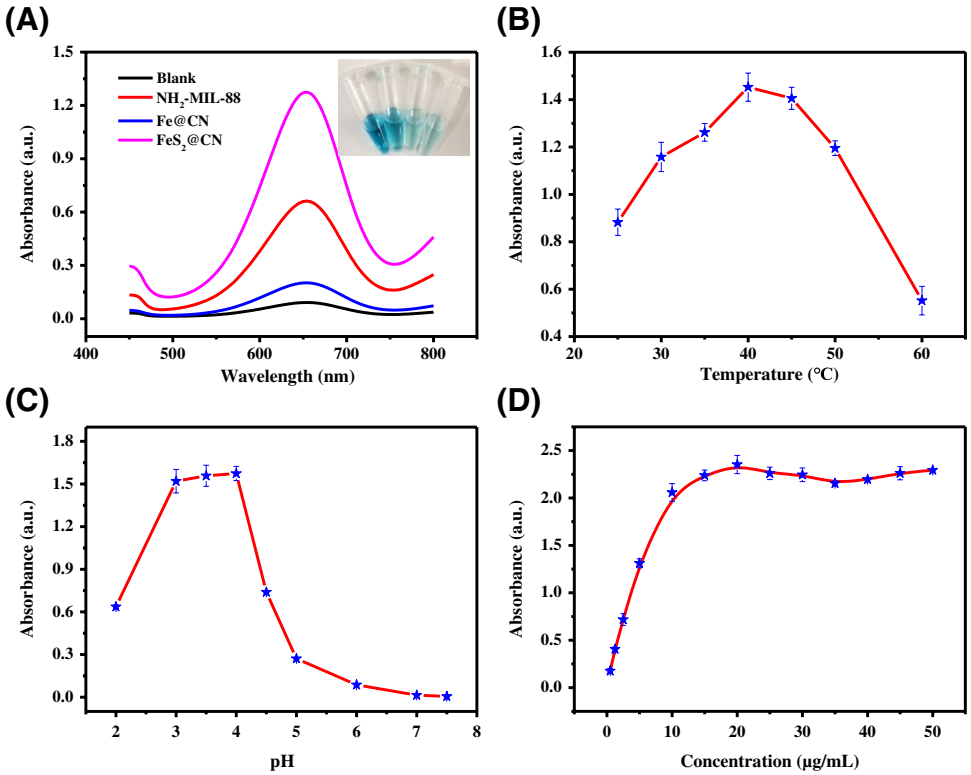

Fig. 4 **A** UV-vis absorption spectra of TMB/H_2O_2 solutions in the presence of different catalysts. The effects of reaction conditions on the peroxidase-like activity of FeS_2@CN: **B** pH; **C** temperature; and **D** FeS_2@CN concentration

Table 1 Comparison of the Michaelis-Menten constants for FeS_2@CN and HRP

Catalyst	Chromogenic substrate	K_m (mM)	V_{max} (10^{-8} Ms^{-1})
FeS_2@CN	TMB	0.018	4.6
	H_2O_2	0.011	8.4
HRP	TMB	0.43	10
	H_2O_2	3.7	8.7

K_m and V_{max} are the Michaelis-Menten constant and maximum velocity, respectively.

Peroxidase-like kinetics and catalytic mechanism of the FeS_2@CN

To identify the steady-state kinetic parameters, we further investigated the catalytic behavior of FeS_2@CN in the presence of H_2O_2 or TMB, which was based on the enzymatic kinetics theory. As elaborated in Fig. S3, typical Michaelis-Menten curves were plotted at varying levels of TMB or H_2O_2 as a substrate. The Michaelis-Menten constants (K_m and V_{max}) were computed based on the double-reciprocal plots. As listed in Table 1, the $K_m(H_2O_2)$ and K_m(TMB) values of FeS_2@CN were much lower than those of HRP, which demonstrated that the as-fabricated nanocomposites had a higher affinity for both chromogenic substrates than conventional HRP [29, 30].

In order to disclose the underlying catalytic reaction mechanisms, we studied the possible active substances in the reaction process through various free radical trapping experiments. Active species including h^+, $\bullet O_2^-$, and •OH can be captured by capturing agents PBQ, EDTA, and IPA, respectively [31]. If three kinds of active species are produced during the catalytic reaction, the absorbance of the catalytic system would decrease after the capture agent was added [32]. As exhibited in Fig. S4A, the absorbance decreased rapidly from 1.05 to 0.07 after IPA was added (Fig. S4A), which offered compelling evidence that •OH played a major role in the reaction process. Meanwhile, a slight decrease in the 652-nm ODs occurred upon the addition of PBQ and EDTA, demonstrating that h^+ and $\bullet O_2^-$ also participated in the catalytic reaction. As a result, the catalytic mechanisms regarding the FeS_2@CN nanozyme are conferred as follows: (1) H_2O_2 molecules are adsorbed on the surface of FeS_2@CN by virtue of multi-interactions and activated to generate •OH by integration with Fe^{2+}. The generated •OH remains stable on the surface of nanocomposites through partial electron exchange or transfer [33]; and (2) TMB is oxidized by •OH to form blue TMBox. The blue color originates from the charge transfer complexes, which are composed of free radicals and TMB [34].

Colorimetric detection of H_2O_2 and glucose based on the FeS_2@CN nanozyme

Under optimized trials, the analytical performance of the as-constructed sensor system for detecting H_2O_2 was evaluated. When the concentration of H_2O_2 increased from 0.5 to 200 µmol/L, the 652-nm absorbance of TMBox increased sharply (Fig. S5A). However, the similar case did not occur, i.e., remaining nearly constant, with further increases in H_2O_2 concentrations from 200 to 800 µmol/L. As a result, a good linear relationship (Y=0.01+0.0085X, R^2=0.9943) was achieved across the concentration range of 0.5–100 µmol/L (Fig. S5B). Correspondingly, the limit of detection (LOD) and limit of quantification (LOQ) for H_2O_2 were calculated to be 0.15 and 0.50 µmol/L, respectively, based on the signal-to-noise ratio (S/N) of 3 and 10. At three fortification levels (5.00, 20.0, and 50.0 µmol/L), the relative recoveries for H_2O_2 spanned the range of 95.2–107% with relative standard deviations (RSDs) of 3.4–5.3% (Table 2) and demonstrated high experimental accuracy. In contrast to other sensors based on nanomaterials, this proposed method offers 3~10-fold lower LOD as compared to the LODs of Co_3O_4 [35], MoS_2 nanosheets [36], and MOF(Co/2Fe) [37]. Moreover, it supplies wider LR than those of other materials, Fe_3O_4@MIL-100(Fe) [38], Co_3O_4 [35], MoS_2 nanosheets [36], and MOF(Co/2Fe) [37] (Table 3).

In the presence of glucose oxidase, glucose can react rapidly with O_2 to produce gluconic acid and H_2O_2 [39]. Because the FeS_2@CN-based system is sensitive to H_2O_2, it can be used to further construct a sensor platform for glucose detection. As the concentrations of glucose increased from 1 to 200 µmol/L (Fig. S6A), the 652-nm ODs increased monotonically with a strong linear correlation (Y=0.02+0.0082X), good linear range (LR, 1-200 µmol/L), and high correlation coefficient (R^2=0.998). Correspondingly, the calculated LOD and LOQ were 0.30 and 1.0 µmol/L, respectively. These performance metrics were compared with several glucose assays by other nanomaterial sensors (Table 3). Evidently, this FeS_2@CN-based sensor achieves 2~4-fold lower LOD than those of Co_3O_4 [35] and MOF(Co/2Fe) [37]. Additionally, it supplied a wider LR than those of Co_3O_4 [35] and MOF(Co/2Fe) [37]. As such, these comparative performance metrics demonstrate that the as-constructed nanozymic sensor is conducive to practical applications in the analytical field of biomolecules in humoral samples.

Selectivity and stability

To evaluate the selectivity and matrix interference of the FeS_2@CN-based colorimetric method for glucose assay, we selected maltose, lactose, and fructose with high concentrations (2 mM), equal to 10-fold as high as the glucose level (0.20 mM), as potential interference biomolecules (Fig. S6B). After the chromogenic reaction, the average 652-nm ODs (n=3) for the three biomolecules were lower than 0.05 a.u., while it reached up to 1.93 a.u. for glucose. This data demonstrates that the colorimetric method based on the FeS_2@CN has high specificity and strong anti-interference capacity for glucose assay.

The stability of the nanocomposite was tested to assess their analytical performance. As illustrated in Fig. S4B, the UV-vis absorption did not vary substantially after a 10-day storing. Therefore, the as-synthesized nanocomposite could be used at least for 10 days in practical applications, demonstrating a good stability in test.

Table 2 The fortified recovery for H_2O_2 based on the colorimetric assay of FeS_2@CN

Samples	Added (µM)	Found (µM)	Recovery (%)	RSDs (%, n=3)
Human serum	No fortification	< LOD	< LOD	< LOD
	5.00	5.34	107	5.3
	20.0	20.5	102	3.4
	50.0	47.6	95.2	3.9

< LOD means < 0.15 µmol/L

Table 3 Comparison of the FeS_2@CN with other nanomaterials for H_2O_2 and glucose assay

Catalysts	H_2O_2		Glucose		Refs.
	LR (µM)	LOD (µM)	LR (µM)	LOD (µM)	
Co_3O_4	1–30	0.77	10-30	0.69	35
MoS_2-nanosheets	5–100	1.5	5-150	1.2	36
MOF(Co/2Fe)	10–100	5.0	/	/	37
Fe_3O_4@MIL-100(Fe)	0.2–30	0.089	/	/	38
FeS_2@CN	0.5–100	0.15	1-200	0.30	This work

LR and LOD denote abbreviations of linear range and limit of detection, respectively.

Table 4 Glucose concentrations detected in human serum samples

Human serum sample	Glucose assay kit (mM)	FeS_2@CN-based colorimetric assay (mM)	RSDs (n=3, %)	Recovery (%)
1	4.63	4.47	3.5	96.0
2	3.43	3.15	3.2	91.8
3	5.20	5.03	5.2	96.7
4	10.3	10.1	4.2	98.0
5	6.50	6.78	2.0	103

Glucose assay in human serum samples

The FeS_2@CN-based nanozymic sensor was used to determine the content of glucose in human serum samples for the sake of exploring its real-world practicability. Each serum sample was diluted 200-fold to ensure the glucose content within the LR. As listed in Table 4, the real glucose contents detected by the present method were in general agreement with those by the glucose assay kit. Correspondingly, satisfactory recoveries for glucose were acquired. Based on this data, we concluded that the FeS_2@CN-based nanozymic sensor has high accuracy and reliability, thereby providing a new alternative for blood glucose assay.

Conclusion

The FeS_2@CN nanocomposite was successfully prepared by varying the synthetic temperatures (300–600 °C) and Fe@CN-to-S ratios (1:3–6) and employed to detect glucose and H_2O_2 by virtue of its peroxidase-like activity. The surface of FeS_2@CN possessed abundant functional groups, and N-doping or S-doping unsaturated/defect sites. The enzymatic kinetics of FeS_2@CN accorded with a typical Michaelis theory owing to promoting the electron transfer between TMB and H_2O_2. The newly developed FeS_2@CN nanozyme assay gave the recoveries of 91.8–103% with RSDs <5.2% for glucose. Thus, the FeS_2@CN-based colorimetric biosensor shows great potential for conventional monitoring of trace-level glucose in humoral samples. However, further research is required to simplify the synthetic procedures for the FeS_2@CN nanocomposite.

Supplementary information The online version contains supplementary material available at https://doi.org/10.1007/s00604-022-05525-w.

Funding This work was jointly supported by the National Science Foundation of China (22076134 and 21876125), Zhejiang Provincial Public Benefit Project (LGC22B070002), Jiangsu Provincial Natural Science Foundation (BK20211338), Key Science & Technology Project of Suzhou City (SS202028), Zhejiang Provincial University Student Sci&Tech Innovation Activity Plan and New Seedling Talent Plan (No. 2021R413061), and National Training Program of Innovation and Entrepreneurship for Undergraduates (202110343068S).

Declarations

Conflict of interest The authors declare no competing interests.

References

1. Bhadra BN, Ahmed I, Kim S et al (2017) Adsorptive removal of ibuprofen and diclofenac from water using metal-organic framework-derived porous carbon. Chem Eng J 314:50–58. https://doi.org/10.1016/j.cej.2016.12.127
2. Deng H, Doonan CJ, Furukawa H et al (2010) Multiple functional groups of varying ratios in metal-organic frameworks. Science 327:846–850. https://doi.org/10.1126/science.1181761
3. Tranchemontagne DJ, Mendoza-Cortés JL, O'Keeffe M et al (2009) Secondary building units, nets and bonding in the chemistry of metal–organic frameworks. Chem Soc Rev 38:1257–1283. https://doi.org/10.1039/b817735j
4. Garibay SJ, Wang Z, Tanabe KK et al (2009) Postsynthetic modification: a versatile approach toward multifunctional metal-organic frameworks. Inorg Chem 48:7341–7349. https://doi.org/10.1021/ic900796n
5. Li Y, Wang LJ, Fan HL et al (2015) Removal of sulfur compounds by a copper-based metal organic framework under ambient conditions. Energ Fuel 29:298–304. https://doi.org/10.1021/ef501918f
6. Li JR, Sculley J, Zhou HC (2012) Metal-organic frameworks for separations. Chem Rev 112:869–932. https://doi.org/10.1002/adma.201705189
7. Farha OK, Spokoyny AM, Hauser BG et al (2009) Synthesis, properties, and gas separation studies of a robust diimide-based microporous organic polymer. Chem Mater 21:3033–3035. https://doi.org/10.1002/adma.201705189
8. Qi Z, Wang L, You Q et al (2017) PA-Tb-Cu MOF as luminescent nanoenzyme for catalytic assay of hydrogen peroxide. Biosens Bioelectron 96:227–232. https://doi.org/10.1016/j.bios.2017.05.013
9. Fu Y, Zhang H, Dai S et al (2015) Glutathione-stabilized palladium nanozyme for colorimetric assay of silver (I) ions. Analyst 140:6676–6683. https://doi.org/10.1039/C5AN01103E
10. Liu S, Lu F, Xing R et al (2011) Structural effects of Fe_3O_4 nanocrystals on peroxidase-like activity. Chem Eur J 17:620–625. https://doi.org/10.1002/chem.201001789
11. Kim JD, Kim M, Kong L et al (2018) Self-anchored catalyst interface enables ordered via array formation from submicrometer to millimeter scale for polycrystalline and single-crystalline silicon. ACS Appl Mater Inter 10:9116–9122. https://doi.org/10.1021/acsami.7b17708
12. Liu Y, Wang C, Yang H et al (2015) Uniformloaded SnS_2/Single-walled carbon nanotubes hybrid with improved electrochemical performance for lithium-ion battery. Mater Lett 159:329–332. https://doi.org/10.1016/j.matlet.2015.07.036

13. Yu S, Jung JW, Kim ID et al (2015) Single layers of WS_2 nanoplates embedded in nitrogen-doped carbon nanofibers as anode materials for lithium-ion batteries. Nanoscale 7:11945–11950. https://doi.org/10.1039/c5nr02425k
14. Xu X, Fan Z, Yu X et al (2014) A nanosheets-on-channel architecture constructed from MoS_2 and CMK-3 for high-capacity and long-cycle-life lithium storage. Adv Energy Mater 4:1400902. https://doi.org/10.1002/aenm.201400902
15. Shao M, Cheng Y, Zhang T et al (2018) Designing MOFs-derived FeS_2@carbon composites for high-rate sodium ion storage with capacitive contributions. ACS Appl Mater Inter 10:33097–33104. https://doi.org/10.1021/acsami.8b10110
16. Sun C, Gradzielski M (2021) Upconversion-based nanosystems for fluorescence sensing of pH and H_2O_2. Nanoscale Adv 3:2538–2546. https://doi.org/10.1039/d0na01045f
17. Xie BB, Yang XH, Zhang RX (2021) Hollow and porous Fe_3C-NC nanoballoons nanozymes for cancer cell H_2O_2 detection. Sensor Actuat B Chem 347:130597. https://doi.org/10.1016/j.snb.2021.130597
18. Cole JB, Florez JC (2020) Genetics of diabetes mellitus and diabetes complications. Nat Rev Nephrol 16:377–390. https://doi.org/10.1038/s41581-020-0278-5
19. Ning D, Liu Q (2019) Luminescent MOF nanosheets for enzyme assisted detection of H_2O_2 and glucose and activity assay of glucose oxidase-ScienceDirect. Sensor Actuat B Chem 282:443–448. https://doi.org/10.1016/j.snb.2018.11.088
20. Zhu N, Zou Y, Huang M et al (2018) A sensitive colorimetric immunosensor based on Cu-MOFs and HRP for detection of dibutyl phthalate in environmental and food samples. Talanta 186:104–109. https://doi.org/10.1016/j.talanta.2018.04.023
21. Zhu XX, Xue Y, Han S et al (2020) V_2O_5-montmorillonite nanocomposites of peroxidase-like activity and their application in the detection of H_2O_2 and glutathione. Appl Clay Sci 195:105718. https://doi.org/10.1016/j.clay.2020.105718
22. Hosseini M, Sabet FS, Kahbbaz H et al (2017) Enhancement of peroxidase-like activity of cerium-doped ferrite nanoparticle for colorimetric detection of H_2O_2 and glucose. Anal methods 9:3519–3524. https://doi.org/10.1039/c7ay00750g
23. Lv SW, Zhao N, Liu JM et al (2021) Newly constructed $NiCo_2O_4$ derived from ZIF-67 with dual mimic enzyme properties for colorimetric detection of biomolecules and metal ions. ACS Appl Mater Inter 13:25044–25052. https://doi.org/10.1021/acsami.1c06705
24. Raizada P, Khan A, Singh P et al (2020) Construction of carbon nanotube mediated Fe doped graphitic carbon nitride and Ag_3VO_4 based Z-scheme heterojunction for H_2O_2 assisted 2,4 dimethyl phenol photodegradation. Sep Purif Technol 247:116957. https://doi.org/10.1016/j.seppur.2020.116957
25. Jin X, Gao S, Wu A et al (2020) Dual-constrained sulfur in FeS_2@C nanostructured lithium-sulfide batteries. ACS Appl Energ Mater 3:10950–10960. https://doi.org/10.1021/acsaem.0c01929
26. Se-Na K, Gwon PC, Kang HB et al (2018) Metal-organic frameworks NH_2-MIL-88(Fe) as carriers for ophthalmic delivery of brimonidine. Acta Biomater 79:344–353. https://doi.org/10.1016/j.actbio.2018.08.023
27. Liu W, Wang YY, Ai ZH et al (2015) Hydrothermal synthesis of FeS_2 as a high-efficiency fenton reagent to degrade alachlor via superoxide-mediated Fe(II)/Fe(III) cycle. ACS Appl Mater Inter 7:28534–28544. https://doi.org/10.1021/acsami.5b09919
28. Liang Y, Bai P, Zhou J et al (2016) An efficient precursor to synthesize various FeS_2 nanostructures via simple hydrothermal synthesis method. CrystEngComm 10:6262–6271. https://doi.org/10.1039/c6ce01203e
29. Wang XX, Wu Q, Shan Z et al (2011) BSA-stabilized Au clusters as peroxidase mimetics for use in xanthine detection. Biosens Bioelectro 26:3614–3619. https://doi.org/10.1016/j.bios.2011.02.014
30. Hu L, Yuan Y, Zhang L et al (2013) Copper nanoclusters as peroxidase mimetics and their applications to H_2O_2 and glucose detection. Anal Chim Acta 762:83–86. https://doi.org/10.1016/j.aca.2012.11.056
31. He YL, Li N, Liu XW et al (2021) 5,10,15,20-tetrakis (4-carboxyl phenyl) porphyrin-functionalized urchin-like $CuCo_2O_4$ as an excellent artificial nanozyme for determination of dopamine. Microchim Acta 188:1–11. https://doi.org/10.1007/s00604-021-04819-9
32. He YL, Li N, Li WK et al (2020) 5,10,15,20-tetrakis (4-carboxylphenyl) porphyrin functionalized $NiCo_2S_4$ yolk-shell nanospheres: excellent peroxidase-like activity, catalytic mechanism and fast cascade colorimetric biosensor for cholesterol-Science direct. Sensor Actuat B Chem 326:128850. https://doi.org/10.1016/j.snb.2020.128850
33. Shi W, Zhang X, He S et al (2011) $CoFe_2O_4$ magnetic nanoparticles as a peroxidase mimic mediated chemiluminescence for hydrogen peroxide and glucose. Chem Commun 47:10785–10787. https://doi.org/10.1039/c1cc14300j
34. Gao L, Wu J, Gao D (2011) Enzyme-controlled self-assembly and transformation of nanostructures in a tetramethylbenzidine/horseradish peroxidase/H_2O_2 system. ACS Nano 5:6736–6742. https://doi.org/10.1021/nn2023107
35. Lu J, Zhang H, Li S et al (2020) Oxygen-vacancy-enhanced peroxidase-like activity of reduced Co_3O_4 nanocomposites for the colorimetric detection of H_2O_2 and glucose. Inorg Chem 59:3152–3159. https://doi.org/10.1021/acs.inorgchem.9b03512
36. Cai S, Han Q, Qi C et al (2015) Pt74Ag26 nanoparticle-decorated ultrathin MoS2 nanosheets as novel peroxidase mimics for highly selective colorimetric detection of H2O2 and glucose. Nanoscale 8:3685–3693. https://doi.org/10.1039/c5nr08038j
37. Hai G, Yang P, Zhang YM et al (2017) A bimetallic (Co/2Fe) metal-organic framework with oxidase and peroxidase mimicking activity for colorimetric detection of hydrogen peroxide. Microchim Acta 184:4629–4635. https://doi.org/10.1007/s00604-017-2509-4
38. Wu YZ, Ma YJ, Xu GH et al (2017) Metal-organic framework coated Fe_3O_4 magnetic nanoparticles with peroxidase-like activity for colorimetric sensing of cholesterol. Sensor Actuat B Chem 249:195–202. https://doi.org/10.1016/j.snb.2017.03.145
39. Jin LH, Shang L, Guo S et al (2011) Biomolecule-stabilized Au nanoclusters as a fluorescence probe for sensitive detection of glucose. Biosens and Bioelectron 26:1965–1969. https://doi.org/10.1016/j.bios.2010.08.019